The Meteoritical Society

Meteoritics & Planetary Science 54, Nr 9, 1930–1950 (2019)
doi: 10.1111/maps.13359

The evolution of polycyclic aromatic hydrocarbons under simulated inner asteroid conditions

Claudia-Corina GIESE[1,2*], Inge Loes TEN KATE[2], Oliver PLÜMPER[2], Helen E. KING[2], Christoph LENTING[3], Yang LIU[2,4,5], and Alexander G. G. M. TIELENS[1]

[1]Leiden Observatory, Faculty of Science, Leiden University, 2300 RA Leiden, the Netherlands
[2]Department of Earth Sciences, Faculty of Geosciences, Utrecht University, 3584 CD Utrecht, the Netherlands
[3]Steinmann-Institut for Geology, Mineralogy und Palaeontology, University of Bonn, 53115 Bonn, Germany
[4]Soft Condensed Matter, Debye Institute for Nanomaterials Science, Utrecht University, 3584 CC Utrecht, the Netherlands
[5]Plymouth Electron Microscopy Centre, University of Plymouth, Devon, PL4 8AA Plymouth, UK
[*]Corresponding author. E-mail: c.c.giese@uu.nl

(Received 12 November 2018; revision accepted 21 June 2019)

Abstract–Large polycyclic aromatic hydrocarbons (PAHs) are an important component of the interstellar medium. PAHs have been identified in the soluble and insoluble matter of carbonaceous chondrites (CCs). Here, we study the evolution of PAHs under conditions relevant to the interiors of asteroids and compare our results to PAHs observed in CCs. We have performed long-term and short-term hydrothermal experiments, in which we exposed PAH-mineral mixture analogs of meteorites to temperature conditions representative of those predicted for asteroids interiors. Our results show that small PAHs with melting points within the aqueous alteration temperature of CCs form carbonaceous spherules in the presence of water. In this work, we describe the microstructure and morphology of these spherules. We discuss the similarities and differences compared to globules isolated from CCs.

INTRODUCTION

Polycyclic aromatic hydrocarbons (PAHs) comprise up to 20% of the carbon material in the interstellar medium (ISM) (Allamandola et al. 1985) with sizes of 50–100 carbon atoms (Tielens 2008). PAHs also represent a significant proportion of the soluble and insoluble organic fraction in carbonaceous chondrites (CCs) (Sephton et al. 1998; Botta and Bada 2002; Sephton 2002). The identified PAHs in CCs range in size from naphthalene (128 amu) to coronene (300 amu) (Becker and Bunch 1997). It has been hypothesized that PAHs from the ISM have been incorporated into solar system bodies, including carbonaceous asteroids during accretion (Plows et al. 2003). We do, however, see a large discrepancy between the size of PAHs detected in the ISM (up to 50–100 carbon atoms; Tielens 2008) and the size of the soluble organic PAHs in carbonaceous meteorites (up to 24 carbon atoms; Sephton 2002). CCs have experienced aqueous alteration, as indicated by the presence of the hydrous minerals like serpentine ($Mg_2Si2O_5[OH]_4$), which is the aqueous alteration product of olivine ($[Mg,Fe]_2SiO_4$). Aqueous alteration affected both the mineralogical composition (e.g., Zolensky 2005; Brearley 2006) and the organic matter (OM) (Bunch and Chang 1980; Herd et al. 2011; Le Guillou et al. 2014; Alexander et al. 2017; Vinogradoff et al. 2018). Here, we study the evolution of PAHs in an aqueous environment under conditions relevant to meteoritic parent bodies, that also includes a possible catalytic effect of olivine serpentinization on OM alteration, as the aqueous alteration of olivine produces significant changes in pH and is known to affect redox conditions in terrestrial samples (Evans et al. 2013). We have conducted two sets of hydrothermal experiments focusing on naphthalene ($C_{10}H_8$), fluoranthene ($C_{16}H_{10}$), and coronene ($C_{24}H_{12}$) with forsteritic olivine used to represent the dominant mineral phase within a meteorite matrix and temperatures ranging from 21 to 150 °C.

Table 1. Overview of carbonaceous chondrite groups, ranging from highly aqueously altered, via primitive (P, nonaltered), to highly thermally metamorphosed.

	Alteration state[a]								
	Aqueous alteration				Thermal metamorphism				
Group	High 1		Low 2	P 3	Low 4	5	6	High 7	Aqueous alteration temperature (°C)[b]	PAHs[c]
CI	■								20–150	Yes
CM	■		■						0–120	Yes
CR	■		■						50–150	Yes
CH				■					n/s	n/s
CB				■					n/s	n/s
CV			■	■					0–150 and 200–340	Yes
CO				■					0–50	Yes
CK				■	■	■	■	■	n/s	n/s

n/s = not specified
[a]Modified after Weisberg et al. (2006).
[b]Modified after Brearley (2006).
[c]Basile et al. (1984); Hahn et al. (1988); Zenobi et al. (1989); Buseck and Hua (1993); De Vries et al. (1993); Clemett et al. (1998); Sephton (2002); Elsila et al. (2005).

EXPERIMENTS

We performed two sets of experiments, long-term hydrothermal experiments (LTHE) and short-term hydrothermal experiments (STHE). The LTHE took place at the Steinmann-Institute for Geology, Mineralogy, and Palaeontology at the University of Bonn and the STHE at the Department of Earth Sciences at Utrecht University. The LTHE aimed to study PAH reactivity in response to the reaction of olivine with water, whereas the STHE focused on the physical alteration of PAHs in an aqueous environment at different temperatures. The LTHE were carried out for 70 days at 150 °C and pressure around 4.8 bar (saturation vapor pressure). Control samples were placed in the dark, at ambient laboratory conditions of 21 °C and atmospheric pressure. The STHE were performed for 20–180 min at 40–150 °C and pressure from 1 to approximately 4.8 bar. The chosen temperature ranges are within calculated aqueous alteration temperature ranges for CCs (Table 1), where 21 °C presents a typical low and 150 °C a typical high temperature for aqueous alteration in PAH-containing CCs (Alexander et al. 2017).

Materials and General Sample Preparation

Three PAHs were used in these experiments, naphthalene ($C_{10}H_8$, 99% purity Sigma-Aldrich), fluoranthene ($C_{16}H_{10}$, 98% purity Sigma-Aldrich), and coronene ($C_{24}H_{12}$, 97% purity Sigma-Aldrich). Due to the toxicity of PAHs, all steps involving PAHs were carried out under a fume hood. Olivine slabs (Fo90, San Carlos quarry, AZ, USA) were cut from olivine single crystals. Before settling on using olivine single crystals in our experiments, we investigated the use of olivine powder. However, as powder is challenging to analyze with SEM and Raman techniques, we did not gain conclusive results from these experiments. The experiments were performed with ultrapure anoxic water that was produced by bubbling argon gas through 500 mL of ultrapure distilled water for up to 12 h using a gas sparger. The transfer of the anoxic water into the reaction vessels was conducted in a glove bag under an argon atmosphere. An argon headspace was created in the reaction vessels by sealing them while still held under argon. Table 2 gives an overview of the physical properties of the PAHs and water that are relevant to our experiments. Care was taken to avoid any contamination by other organic materials during all stages of sample preparation and handling. The olivine slabs were cut into 4 mm × 5 mm × 2 mm pieces and were not polished. No organic containing solvents were used during cutting. After cutting, the olivine surfaces were cleaned with ethanol to remove olivine dust and potential organic contamination. All equipment was autoclaved and cleaned with ethanol before use. The polytetrafluoroethylene (PTFE) liners for the hydrothermal autoclaves and their lids (Fig. 1) were cleaned with ethanol, followed by nitric acid solutions. Ethanol is a highly volatile solvent and thus is not expected to leave an organic residue on the equipment. Autoclaved, single-use pipette tips were chosen when pipettes were needed. Sample material was stored in sealed amber-colored glass vials that were placed in a closed box. For short-term storage of a few hours, the

Table 2. Physical properties of naphthalene, fluoranthene, coronene, and anoxic water relevant for the experiments.

	Anoxic water H_2O	Naphthalene $C_{10}H_8$	Fluoranthene $C_{16}H_{10}$	Coronene $C_{24}H_{12}$
Purity (%)	n/s	99	98	97
Supplier	–	Sigma-Aldrich	Sigma-Aldrich	Sigma-Aldrich
Average mass (Da)	18.015	128.171	202.251	300.352
Melting point (°C) at 1.01 bar	0	80–81[a,b]	107–109[a,b]	438–439[a,b]
Boiling point (°C) at 1.01 bar	100	217–218[a,b]	383–384[a,b]	525[b], 590[a]
Pressure (bar) at 150 °C	4.77[c]	n/s	n/s	n/s
Solubility (g L^{-1}) in water at 25 °C/1 bar	–	0.031[b]	0.003[b]	1×10^{-7}[b]
Solubility (g L^{-1}) in water at 1 bar	–	0.244 (73 °C)[b]	0.017 (60 °C)[b]	n/s
Density (g cm^{-3}) at 20 °C/1 bar	0.99[c]	1.02[d]	1.18[e]	n/s
Density (g cm^{-3}) at 150 °C/1 bar	0.91[c]	0.92[f]	n/s	n/s

n/s = not specified.
[a]Karcher (1988).
[b]Yalkowsky et al. (2010).
[c]Kell (1975).
[d]Auwers and Frühling (1921).
[e]Fiedler et al. (1997).
[f]Chirico et al. (1993).

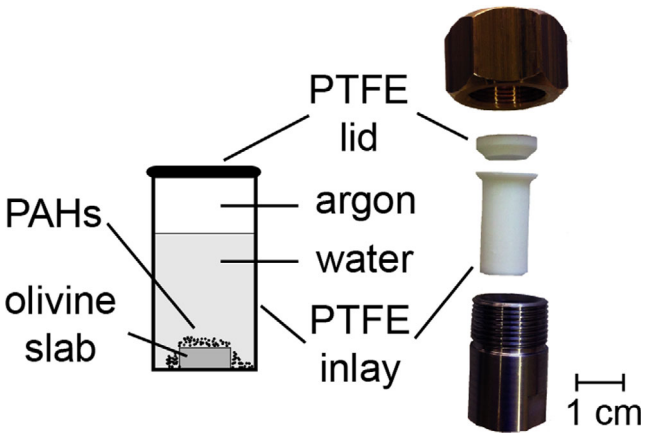

Fig. 1. The LTHE sample holder: a 2 ml PTFE lined steel hydrothermal autoclave reactor. (Color figure can be viewed at wileyonlinelibrary.com.)

samples were stored at room temperature. However, for long-term storage, the samples were placed in a refrigerator at 4 °C.

Long-Term Hydrothermal Experiments

Three types of samples were used in the long-term experiments, PAH–olivine samples in water, PAH in water, and olivine in water. Table 3 gives an overview of the number of experiments per compound, the substrate, and the composition of the headspace. Two sample preparation methods were used for the PAH–olivine samples. In the first method, 10 mg of PAH was dissolved in 1 mL toluene ($C_6H_3CH_3$ for liquid chromatography LiChrosolv®, purity >99%). Naphthalene and fluoranthene were dissolved fully, and coronene powder was used in suspension. The PAH-toluene solution was applied dropwise and uniformly onto the olivine slab surface, whereby each drop was allowed to dry before further application of fluid droplets. The drops were applied on the largest olivine surface in as small a quantity as possible to avoid the solution running off the slab. FT-IR analysis of dry PAH-toluene suspension showed no residue of toluene on the olivine after drying. The PAH-coated olivine slab was transferred into the 2 mL PTFE-inlay, which was already inserted into the steel container, with the coated surface facing upward so that the largest area was exposed to the solution. Figure 1 shows the stainless steel, PTFE-lined reaction vessel. The reaction vessel with the coated olivine was then placed into a glove bag, and the glove bag was sealed. After filling the glove bag with argon to create an anoxic atmosphere, 1.5 mL of anoxic water was added to each of the reaction vessels, which were then sealed using a PTFE lid and steel cap. The resulting water–PAH ratio was 15:1 by mass. For the second method, the olivine slab was placed into a reaction vessel; 10 mg of PAH powder was placed on top of the olivine crystal followed by 1.5 mL of anoxic water. This mixture led to the same water–PAH ratio of 15:1 by mass and a water–rock ratio of 6:1 by mass with ~56 mm^2 surface of the olivine exposed within the experiment. We chose a higher water–rock ratio than probably expected in a meteorite to simulate water-saturated conditions, reducing the possibility of the reaction being limited due to lack of water. However, our chosen water–rock ratio still lies within the limit of water to rock ratios described as closely matching the gross characteristics for the aqueous alteration of carbonaceous meteorites (Schulte and Shock 2004; Brearley 2006). After filling, the reaction vessels were

Table 3. List of LTHE experiments, showing the number of experiments per compound, the substrate, and the composition of the headspace.

				Head space			
				Argon		Air	
Compound	Number of experiments	Substrate		21 °C	150 °C	21 °C	150 °C
Naphthalene	15	None	5	–	1	2	2
		Olivine slab	10	5	5	–	–
Fluoranthene	16	None	6	1	1	2	2
		Olivine slab	10	3	5	1	1
Coronene	8	None	5	1	–	2	2
		Olivine slab	3	1	2	–	–
Olivine	14	Olivine slab	6	2	2	1	1

divided into two groups. The first group was placed in an oven that was purpose-built in-house at the Steinmann-Institute for Geology, Mineralogy and Palaeontology of the University of Bonn and heated to 150 °C for 70 days. The other group was placed in a room with a stable temperature of 21 °C for the same period of time. After the experiments, the reaction vessels were allowed to cool for several hours before being placed into the glove bag and opened under an argon atmosphere. First, the liquid phase was removed with a manual microliter pipette and transferred to an amber-colored glass vial. Care was taken to remove the liquid; however, in some reaction vessels, not all the fluid could be removed. Then, the olivine slab and PAH residue were removed using tweezers or a spatula and placed in a second amber-colored glass vial. An amber-colored glass vial was selected to protect the samples from photochemical reactions.

Short-Term Hydrothermal Experiments

Short-term experiments of naphthalene, fluoranthene, and coronene crystals in anoxic water at temperatures up to 150 °C were carried out in a conventional laboratory oven (Memmert UF110, universal drying and baking oven) at the Department of Earth Sciences at the Utrecht University. Each PAH was tested in a separate experiment series. Each experiment series consisted of 18 1.5 mL glass vials filled with 6.7 mg of the PAH being examined. These vials were separated into two sets, where 1 mL of ultrapure anoxic water was added to one set of the vials (water–PAH ratio 15:1 by mass). The anoxic water was prepared in the same way as the LTHE. Argon gas was then flushed into the headspace, and the vials were sealed with a septum. The filled vials were placed on aluminum foil, which lay loosely on a metal grid before being placed into the oven to avoid direct contact with the oven surface and to ensure homogeneous heating. Once all the vials were secured within the oven, the temperature of the oven was increased from room temperature (21 °C) to 40 °C. The start of the first experiment was taken as the time that the oven had stabilized its temperature. After 20 min at 40 °C, one vial of PAH with water and one vial of PAH without water were carefully and quickly removed from the oven and immediately photographed. This resulted in very little change in the temperature within the oven. The oven was then heated to 60 °C, and the next experiment initiated once the temperature had stabilized again. This procedure was repeated every 20 °C between 60 and 150 °C, removing two vials with each temperature step until all 18 vials had been removed from the oven. Vials that had been removed and photographed were allowed to cool beside the oven so that changes related to cooling could be monitored. Once all vials had cooled to room temperature, the liquid phase was removed using a manual microliter pipette and transferred to an amber-colored glass vial. The PAH residues were removed, when possible, using a spatula and placed in a glass vial. No glove bag was used in these experiments. After the experiments, all samples were stored using the same procedures as the LTHE.

Raman Spectroscopy

The Raman spectroscopic analyses took place at the different locations of the experiments, that is, University of Bonn and Utrecht University, to guarantee analysis of the samples as quickly as possible after the end of experiments. Raman spectra of LTHE samples were obtained with a high-resolution Horiba Scientific HR800 Raman spectrometer equipped with an Olympus BX41 microscope, He-Ne (632 nm) and near infrared (785 nm) laser, and an electron-multiplier charge-coupled device (CCD) detector. The acquisition time of each spectrum was 6–15 s with a maximum of 20 iterations. Measurements used a grating of 600 grooves per mm. The Horiba Scientific HR800 Raman spectrometer is located at the Steinmann-Institute for

Geology, Mineralogy and Palaeontology of the University of Bonn.

Raman spectra of STHE samples and the initial sample material were obtained with a WITec 300 alpha Raman spectrometer with a built-in light microscope, and equipped with Nd:YAG (532 nm) and near infrared (785 nm) lasers and CCD detectors optimized for the different wavelengths. The acquisition time was 0.05–0.5 s with a maximum of five iterations. All samples were measured with a grating of 600 grooves per mm. The WITec 300 alpha Raman spectrometer is located at the Department of Earth Sciences, Utrecht University.

All coronene samples were measured with a 785 nm laser with both the Horiba and WITec Raman spectrometers. Fluoranthene and naphthalene crystals were both measured with a 632 nm laser at the Horiba and 532 nm laser at the WITec Raman instrument, where fluoranthene samples were measured at reduced laser intensity to prevent sample burning. All Raman spectra were analyzed after baseline correction and by fitting the spectra to Lorentzian or Gaussian line shapes.

Focused Ion Beam-Scanning Electron Microscopy

Solid samples were mounted on an aluminum stub using double-sided, conductive copper tape (purchased from VWR) and coated with platinum-palladium alloy to a thickness of 10 nm. A selected suite of solid samples was investigated using a focused ion beam scanning electron microscope (FIB-SEM; FEI Helios Nanolab G3 UC) equipped with an energy-dispersive X-ray spectroscopy (EDX) system. Overview images of the material were taken using acceleration voltages between 0.1 and 5 kV to avoid charging effects and recrystallization of the organic material under the electron beam. Lower acceleration voltages allowed higher resolution images to be taken of the surface features as the interaction volume is minimized. The focused ion beam capability of the FIB-SEM was used to acquire a slice-and-view series for 3D volume reconstructions. Prior to all FIB operations, a platinum strip of 2 μm thickness was deposited to shield the rest of the sample from ion beam damage. For cross-sectioning, a Ga-FIB was used at 30 kV and 0.43 nA. Images of the cross-sectioned surface were obtained using the backscattered electron mode at 15 kV and 0.4 nA with a voxel size of 8.33 × 8.33 × 20 nm. No alteration of the material's microstructure due to the electron beam was observed during continuous imaging at this kV. The FIB-SEM nanotomography volume was reconstructed and analyzed using the FEI Avizo 9 software. A detailed explanation of the FIB-SEM for milling materials can be found in Liu et al. (2016).

We performed calculations based on heat conduction models to assure that we have not altered our samples during their interaction with the ion beam in FIB-SEM investigations. Following Volkert and Minor (2011), the increase in temperature T for an incoming ion beam can be simplified to $T = P/(\pi \times a \times \kappa)$, where a is the radius of the circular ion beam profile on the sample surface, κ the thermal conductivity of an organic crystal, and P is the ion beam power in Watts. Using an ion beam acceleration voltage of 30 kV, a beam current of 0.43 nA, a sample thickness of 10 μm, and a very low thermal conductivity of 0.1 W $m^{-1} \times K$ (adequate to describe κ of PAHs; Ross et al. 1979), one obtains a temperature increase of 4 K. A more complex model published by Ishitani and Yaguchi (1996) results in a temperature increase of approximately 16 K. Both results are much lower than any melting temperature of the investigated PAHs. Moreover, scan durations during individual ion beam treatments were less than a few milliseconds. Thus, together with a minimal heating effect by the ion beam, we infer that the FIB-SEM conditions used are adequate for morphological investigations of PAHs.

RESULTS

Long-Term Hydrothermal Experiments

Extracted Fluids

Fluids extracted from the hydrothermal experiments with naphthalene and fluoranthene at 150 °C exhibit a yellow to brownish coloration. In contrast, fluids from experiments with coronene, pure and with olivine, and experiments with solely olivine (no PAH) at 150 °C, as well as all experiments left at 21 °C, did not exhibit a discoloration of the fluid.

Baseline Hydrothermal Experiments: PAHs in Water and Olivine Crystal in Water

Naphthalene, fluoranthene, and coronene crystals submerged in water at 21 °C for 70 days did not show any macroscopic alteration and remained present at the bottom of the PTFE reactor. In contrast, after treatment at 150 °C, only coronene remained visible within the PTFE reactor, whereas naphthalene and fluoranthene crystals could no longer be distinguished macroscopically.

In order to separately evaluate the reaction of olivine with water at 21 and 150 °C, we conducted baseline experiments using slabs of olivine submerged in anoxic deionized water in the absence of PAHs. Olivine slabs from experiments at 21 °C did not exhibit any macroscopic alteration or changes in color, whereas olivine slabs placed at 150 °C show surface

discoloration, changing from the original olive green color to light or dark brown.

PAHs with Olivine in Water

Hydrothermal PAH alteration experiments with olivine show that at 21 °C naphthalene, fluoranthene and coronene crystals remain unaffected and do not exhibit any macroscopic alteration features. The added olivine crystals from experiments with PAHs at 21 °C also do not show signs of discoloration suggesting an alteration.

At 150 °C, macroscopically visible naphthalene and fluoranthene crystals disappear, and a dark colored layer largely covers the olivine crystal surfaces (see Figs. 2d and 2f). In contrast, in experiments with coronene, crystals could still be observed lying on the olivine surfaces without any visible signs of alteration. The olivine slabs themselves display an intense discoloration to a dark brown color.

The most notable feature of all naphthalene and fluoranthene experiments at 150 °C is the occurrence of nm- to μm-sized spherules seen on top of the olivine substrate in the SEM (Figs. 3 and 4). These spherules are distributed across the entire olivine slab surface and display a variety of morphologies. However, in experiments with PAHs without olivine and coronene with olivine, no spherules were seen.

Carbonaceous Spherules

Spherules formed during naphthalene-olivine alteration experiments at 150 °C range in diameter from 0.04 to 0.47 μm and are arranged to form 120° interface angles. The spherule size distribution is in agreement with a lognormal cumulative probability distribution (Fig. 5c) and differed only minimally between duplicate experiments (compare Figs. 3a and 3b). In some minor cases, spherule–spherule interactions led to the distortion of the spherical shape. Cross-sectional imaging of the spherules using FIB-SEM–assisted nano-milling reveals that the naphthalene-derived spherules are homogenously solid and do not exhibit any distinctive internal microstructures (Figs. 3c and 3d). This is in contrast to spherules formed during the fluoranthene-olivine experiments at 150 °C (Figs. 4a, 4g, and 4i). Spherules formed during these experiments are substantially larger and range in size from 20 to 50 μm. However, several smaller spherules (0.5–5 μm) can be found surrounding the largest spherules (Fig. 4a). The size distribution of these spherules reflects an asymptotic size cumulative probability distribution (Fig. 5d). In addition, plate-shaped organic material can be found to form either directly on the olivine surface or the surface of large spherules (Figs. 4a and 4d). FIB-SEM cross-sectioning revealed a variety of internal microstructures. The shape of the largest spherules arises due to a double layer structure that homogeneously surrounds a more complex internal structure. The outer layer has a thickness of around 0.03 μm and the inner layer from around 0.06 μm. The internal structure displays a complex arrangement of isolated pockets that exhibits precipitates, which resemble a dendritic structure (Figs. 4b, 4c, and 4f). The dendrites vary in thickness and appear to start randomly from the inner rim. In contrast, the intermediate-sized spherules with a size of ~5 μm and those smaller than 5 μm are internally hollow (Figs. 4g, 4h, and 4i).

Chemical Analysis

The microscopic alteration behavior of naphthalene on an olivine slab at 21 °C could not be investigated due to the quick evaporation of naphthalene in the SEM vacuum chamber. Although analysis of naphthalene from the LTHE at 21 °C was not possible with the SEM, Raman spectra could be obtained from duplicate samples. The obtained spectra are identical to those of initial naphthalene crystals (Fig. 2; Table 4).

All spherules formed at 150 °C in LTHE with naphthalene appear to have a lower vapor pressure than the starting material. Naphthalene visibly evaporated within hours when exposed to air in the laboratory or within minutes in the SEM vacuum, whereas the newly formed spherules showed no change in appearance even up to a year after the experiment. Similarly, the original fluoranthene material evaporated within hours of exposure to air in the laboratory, but the spherules produced during the fluoranthene experiments did not exhibit any changes in size or external appearance. The EDX spectra of the spherules show only C, although H may also be present in the material as this is not detectable using SEM-EDX.

Olivine slabs from LTHE at 150 °C in water with and without the presence of PAHs experienced a color change. SEM-EDX and Raman spectroscopic analysis indicate that the different color is caused by the presence of hematite (Fe_2O_3; Fig. 2o). Figure 2 shows the Raman spectra of naphthalene, fluoranthene, and coronene in comparison to their initial spectra, and in Table 4, the determined band positions with full width half maximum values (FWHM) are summarized. Crystals from LTHE with coronene at 150 °C in water with and without the presence of olivine indicate no signs of chemical alteration, which is in agreement with the chemical analysis of samples from LTHE experiments at 21 °C (Fig. 2i; Table 4). However, fluoranthene and naphthalene from LTHE at 150 °C in water showed evidence for chemical changes in the Raman spectra (Figs. 2a and 2b; Table 4), linked to their transformation from crystals to spherules, both in the presence of olivine, but, also in the absence of olivine. Unfortunately, fluorescence was often a problem when analyzing the

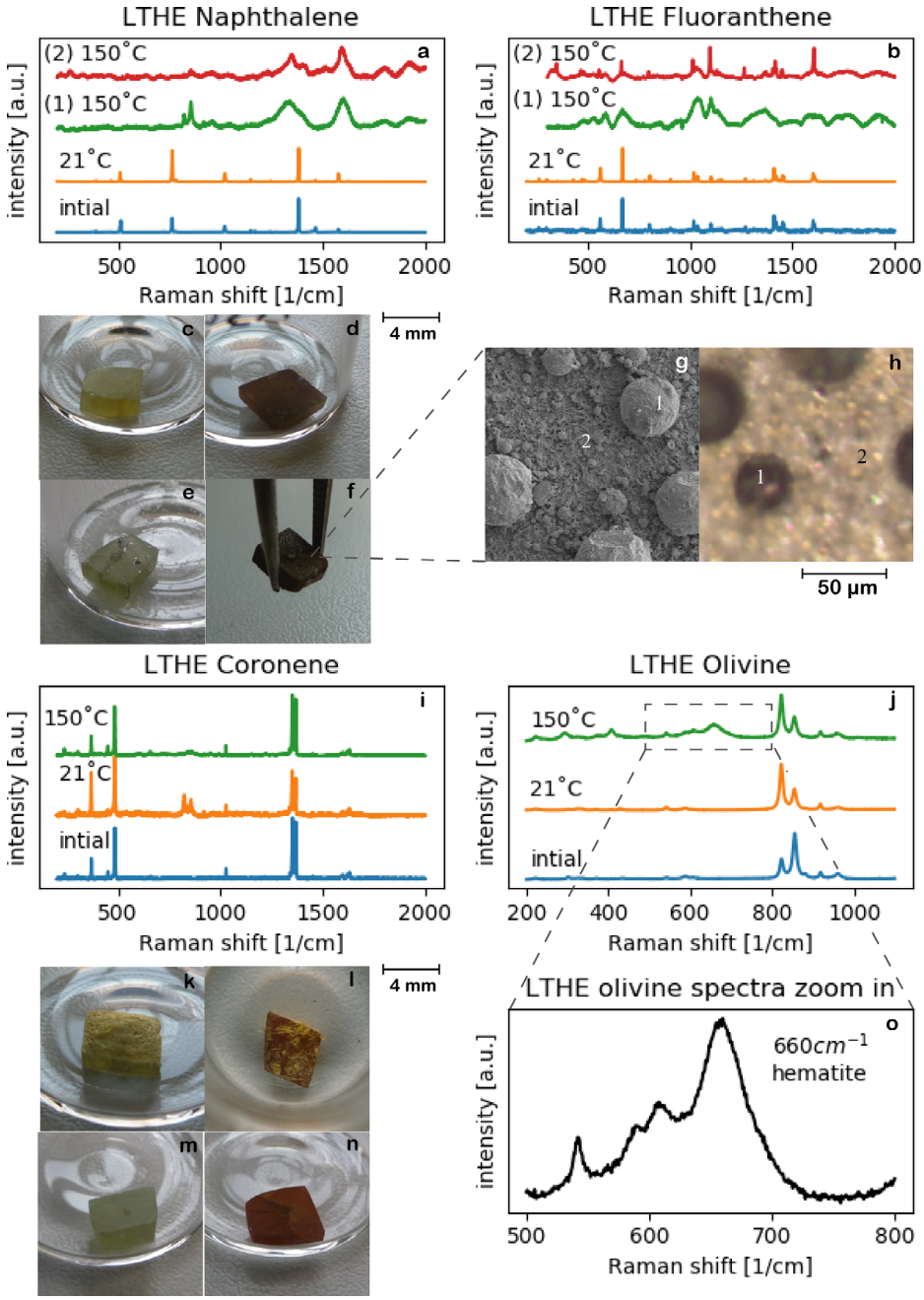

Fig. 2. Raman spectra and corresponding LTHE samples. a, b) Raman spectra of naphthalene and fluoranthene exposed to water and different temperatures (21 °C or 150 °C) in comparison with initial spectra. There are two spectra each of naphthalene and fluoranthene samples at 150 °C. c) Olivine slice with naphthalene exposed to water at 21 °C in LTHE. d) Olivine slice with naphthalene exposed to water at 150 °C in LTHE. e) Olivine slice with fluoranthene exposed to water at 150 °C in LTHE. f) Olivine slice with fluoranthene exposed to water at 150 °C in LTHE. g) SEM image of globules formed on olivine slice in LTHE with fluoranthene (e). The numbers (1; 2) in the image correspond to Raman spectra of fluoranthene exposed to water at 150 °C in LTHE (b). h) Microscopy image of globules formed on olivine slice in LTHE with fluoranthene (e). The numbers (1; 2) in the image correspond to Raman spectra of fluoranthene exposed to water at 150 °C in LTHE (b). i) Raman spectra of coronene after exposed to water and different temperatures (21 °C or 150 °C) in comparison with initial spectra. j) Raman spectra of olivine after exposure to water and different temperatures (21 or 150 °C) in comparison with initial spectra. k) Olivine slice with coronene exposed to water at 21 °C in LTHE. l) Olivine slice with coronene exposed to water at 150 °C in LTHE. m) Olivine slice to water at 21 °C in LTHE. n) Olivine slice exposed to water at 150 °C in LTHE. o) Zoom into olivine spectra exposed to water at 150 °C in LTHE (j). The zoom-in shows a spectrum with a hematite peak. (Color figure can be viewed at wileyonlinelibrary.com.)

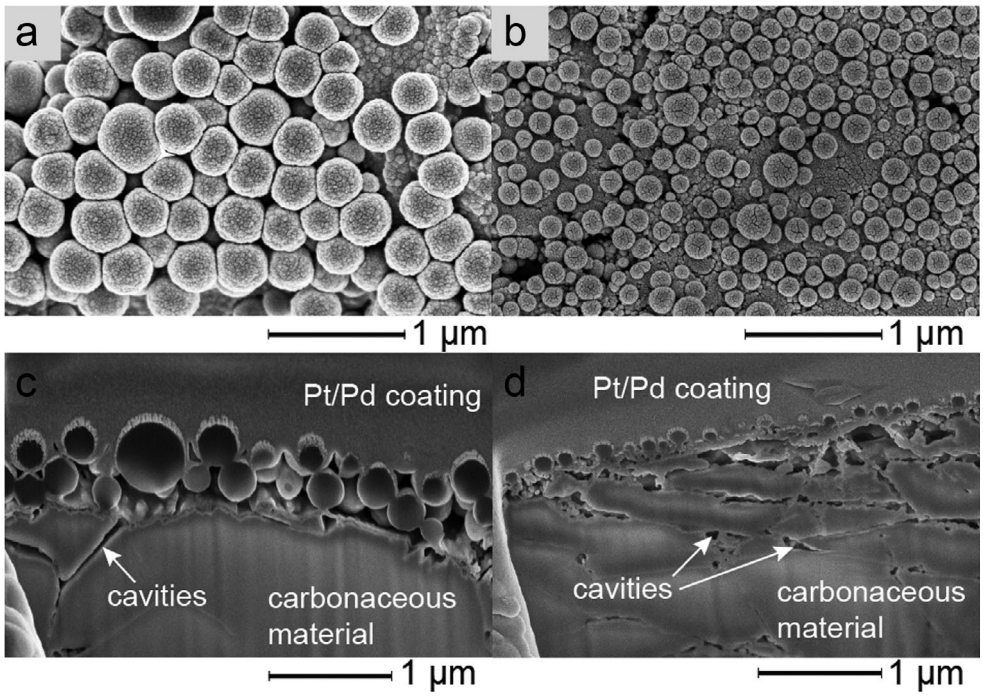

Fig. 3. LTHE with naphthalene on single crystal olivine at 150 °C. a) SEM images of samples from two experiments, (c) show nano carbonaceous globules formed over the entire olivine surface. Globule diameter varies by around 200 nm between separate experiments. Corresponding cross sections (b), (d) reveal that the globules have a solid internal structure. Below the globules, a solid carbonaceous layer is present that contains cavities.

spherules even with reduced laser power resulting in only a few useable spectra being obtained from these samples. The new Raman modes of the spherules measured in the naphthalene LTHE at 150 °C correspond to C=C stretching (1586 cm^{-1}, 1596 cm^{-1}, 1799 cm^{-1}) or C–C ring vibration (1324 cm^{-1}), thus can still be assigned to an aromatic compound (Lin-Vien et al. 1991). This is consistent with an absence of elements such as O or N in the EDX spectra from the SEM, which would indicate the incorporation of a new functional group into the PAH due to aqueous alteration. The Raman bands 823 cm^{-1} and 855 cm^{-1} to 856 cm^{-1} belong to the underlying olivine sample. The FWHM mean values of the new bands from LTHE with naphthalene at 150 °C are up to 24 times broader in comparison to the initial naphthalene crystals and the bands from LTHE at 21 °C. The fluoranthene spectra still contain a Raman band that can be assigned to C–C stretching (1102 cm^{-1}; Lin-Vien et al. 1991) of the initial fluoranthene spectrum. The FWHM mean value of the resolvable band from LTHE with fluoranthene at 150 °C is two (150-2) to four (150-1) times broader in comparison to the initial fluoranthene spectrum. The Raman spectra do not directly correlate with specific, cataloged organic molecules, such as functionalized or other PAHs (e.g., Ram et al. 1983; Colangeli et al. 1992; Schaeffer et al. 1995; Shinohara et al. 1998; Alajtal et al. 2010; Tan et al. 2017). Therefore, we were not able to identify any specific reaction products based on the Raman spectra. The broadening of the Raman bands centered at the same wave number as the original PAH could indicate a loss of crystallinity (similar to, e.g., metamictization in zircons; Nasdala et al. 1995) consistent with the formation of different morphology and change in vapor pressure of the PAH solids in these experiments. Alternatively, the broad bands could be an agglomeration of many, smaller, sharper bands that lie at similar wave numbers representing a mixture of molecules with similar chemical groups.

Short-Term Hydrothermal Experiments

Macroscopic Observations

Figure 6 summarizes the macroscopic observations of all STHE. In the experiments with naphthalene powder, the majority of the powder was observed to float at the water–gas interface at 21 °C. Only a small amount of crystals settled at the bottom of the glass vessel. Increasing the temperature to 70 °C, just below the melting point (see Table 2) of naphthalene resulted in no visible change in the naphthalene powder or the aqueous phase. However, increasing the temperature to

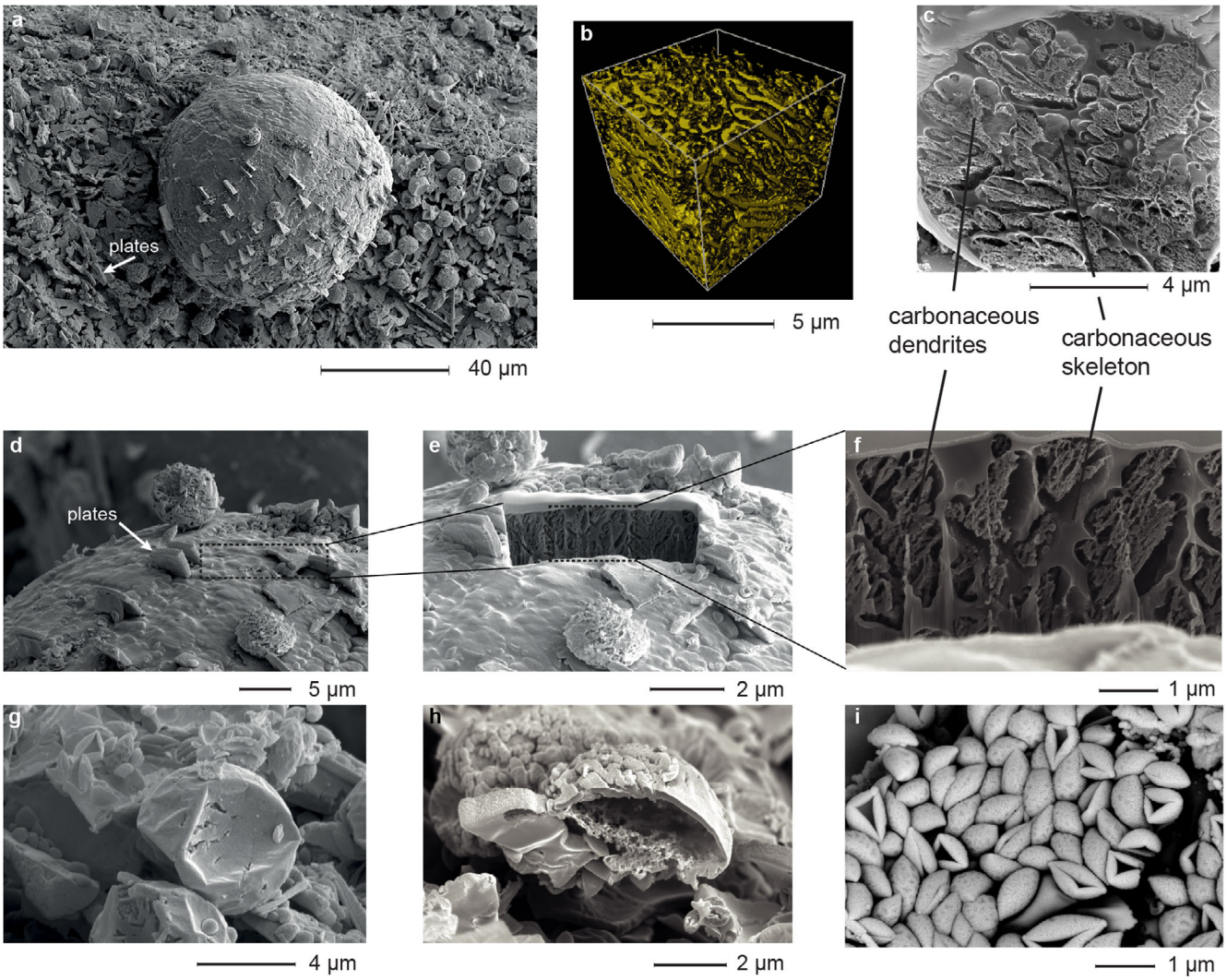

Fig. 4. LTHE with fluoranthene on solid olivine at 150 °C. A variety of carbonaceous globules formed in LTHE with fluoranthene and olivine in water at 150 °C. a, g, and i) represent three types of globules formed in one experiment. These three types differ in both size and surface area density. a) An example of the largest globules (15–50 µm). This type of globule has a distinctive internal structure, as shown in (b), (e), and (f). b) A three-dimensional reconstruction of the internal morphology of a globule, built up from slices as shown in (c), revealing the presence of carbonaceous dendrites and a carbonaceous skeleton. d) The area where a FIB cross section was made. e and f) Magnified views into the cross section showing similar internal structure as shown in (b). g and h) Two medium-sized (Ø 5 µm) hollow globules. i) The smallest globules with a deflated appearance. (Color figure can be viewed at wileyonlinelibrary.com.)

90 °C, 10 °C above the melting point of naphthalene caused an apparent visible change in naphthalene's behavior. Naphthalene crystals were no longer observed at the air–water interface. Instead, an immiscible fluid was observed floating at the air–water interface, and aggregated 2–3 mm sized droplets were found within the fluid at the bottom of the experimental vessel. Increasing the temperature to 100 °C, 20 °C above the melting point, resulting in the occurrence of 1 mm droplets found floating at the water–gas interface and the overall solution becoming cloudy. Just a few droplets formed at lower temperatures were still observable at the bottom of the experimental vessel. Above 120 °C, the size of droplets decreases with rising temperature until the droplets were no longer visible by eye, the concave meniscus disappeared, and only a cloudy emulsion remained. The cloudy emulsion persisted during the temperature increase. At 150 °C, 70 °C above the melting point of naphthalene, the fluid became clear again without any indication of other phases present within the vessel.

Short-term experiments conducted with fluoranthene showed similar behavior as the naphthalene experiments when the higher melting point of fluoranthene (107–

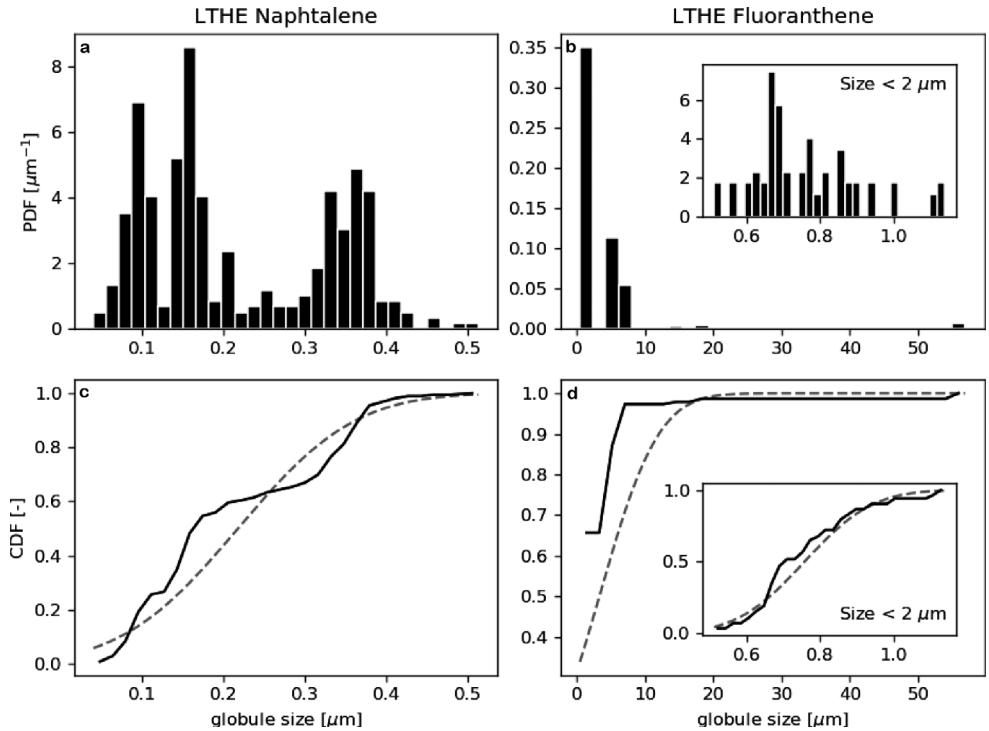

Fig. 5. Histogram (probability density function: PDF) and cumulative distribution function (CDF) of the size of globules formed in long-term experiments (LTHE) with naphthalene and fluoranthene. a) Histogram of globules size formed during naphthalene LTHE. b) CDF showing the globule size distribution from naphthalene LTHE. a, b) The distribution of globules sizes in the naphthalene LTHE indicates a homogenous growth. c). Histogram of globules size formed of fluoranthene LTHE. d) CDF showing the globule size distribution of fluoranthene LTHE. c, d) The distribution of globules sizes in the fluoranthene LTHE indicates a heterogeneous growth. Only the small-sized globules (size <2 μm) formed during fluoranthene LTHE indicate a homogenous growth. The histograms and CDFs are based on around 380 globules (black line) and have an arithmetic mean of 0.22 μm for naphthalene and 3.33 μm for fluoranthene with a SD of 0.11 and 6.82 μm, respectively (gray dashed line).

109 °C) was exceeded (Table 2). Before the melting point, fluoranthene crystals did not change their appearance. At 120 °C, 10 °C above the melting point, an immiscible fluid was formed at the air–water interface as well as aggregated 2–3 mm sized spherules. At 140 °C, 30 °C above the melting point, no spherules were visible in the fluid floating at the fluid–air interface or the bottom of the experiment vessel. Instead, only the immiscible fluid at the fluid–air interface, forming a concave meniscus, was present and the rest of the fluid in the vessel appeared cloudy. At 150 °C, 40 °C above the melting point the fluid remained cloudy with the immiscible fluid floating at the air–water interface. However, after the solution cooled, the fluid becomes clear again, without any indication of other phases present within the fluid. The immiscible fluid at the air–water interface solidified into a very thin layer on top of the aqueous phase.

In water-absent experiments with naphthalene and fluoranthene under an argon atmosphere, PAHs were observed to form a melt immediately around the PAH melting point. Before melting, the naphthalene powder was present as an aggregated lump, whereas the fluoranthene remained as individual crystals. After the melting point of naphthalene and fluoranthene was exceeded, both PAHs formed a single fluid layer on the bottom of the glass vials.

In the coronene experiments both with and without anoxic water, no difference in the appearance of the coronene crystals or the water was observed within the temperature range tested (21–150 °C).

Ex situ Observations

After the STHE, the remaining visible residues of naphthalene and fluoranthene were present as a floating phase and spherules located on the bottom of the experimental vessel. Upon quenching, the floating PAH (naphthalene or fluoranthene) liquid phase solidified and sank. As a result, we were unable to separate the PAH (naphthalene or fluoranthene) material from the air–water interface and the bottom of the glass reaction vessel. SEM images (Figs. 7 and 8) were obtained for a representative suite of the solid residues retrieved from the STHE with naphthalene and fluoranthene. In the STHE coronene experiments, coronene crystals sank to

Table 4. Determined peak position (±3 cm^{-1}) and full width half maximum values for the initial PAHs used in the experiment in comparison with samples from LTHE at 21 °C and two samples from 150 °C experiments, where the two peaks of 150 °C are representative for each sample. Coronene samples from LTHE at 150 °C do not vary.

Coronene						
Lit.[a]	Initial		21 °C		150 °C	
Peak	Peak	FWHM	Peak	FWHM	Peak	FWHM
371	368	2.53 ± 0.09	367	3.44 ± 0.36	368	2.55 ± 0.33
488	483	5.00 ± 0.24	483	5.61 ± 0.42	484	5.45 ± 0.39
1028	1026	2.83 ± 0.18	1026	3.94 ± 0.43	1026	3.08 ± 0.40
1352	1351	4.35 ± 0.12	1350	6.03 ± 0.25	1350	4.68 ± 0.19
1370	1368	3.41 ± 0.11	1367	4.33 ± 0.25	1368	3.51 ± 0.17
1618	1617	10.90 ± 1.09	1617	12.75 ± 1.54	1617	10.20 ± 1.06
1632	1628	4.64 ± 0.34	1629	5.02 ± 0.52	1629	5.62 ± 0.48

Fluoranthene								
Lit.[b]	Initial		21 °C		150 $°C^{-1}$		150 $°C^{-2}$	
Peak	Peak	FWHM	Peak	FWHM	Peak	FWHM	Peak	FWHM
670	669	2.33 ± 0.10	670	2.25 ± 0.08			664	2.94 ± 0.19
1018	1017	2.93 ± 0.21	1018	2.74 ± 0.05			1013	3.31 ± 0.24
1102	1102	3.52 ± 0.25	1102	3.15 ± 0.06	1101	20.20 ± 1.26	1097	4.63 ± 0.17
1270	1269	3.84 ± 0.72	1270	3.79 ± 0.16			1264	4.96 ± 0.26
1410	1410	3.87 ± 0.32	1409	3.86 ± 0.15			1404	3.21 ± 0.71
1420	1421	5.46 ± 0.76	1420	4.50 ± 0.44			1416	6.44 ± 0.54
1453	1452	4.06 ± 0.67	1452	4.49 ± 0.31			1447	5.02 ± 0.30
1608	1606	4.56 ± 0.99	1611	2.43 ± 0.28			1606	3.43 ± 0.17
3053	3053	10.43 ± 1.04	3053	11.90 ± 0.11			3050	12.31 ± 0.76

Naphthalene								
Lit.[b]	Initial		21 °C		150 $°C^{-1}$		150 $°C^{-2}$	
Peak	Peak	FWHM	Peak	FWHM	Peak	FWHM	Peak	FWHM
513	512	2.19 ± 0.10	509	2.86 ± 0.12				
763	762	3.26 ± 0.09	763	3.24 ± 0.07				
					[c]823	9.79 ± 0.44		
					[c]855	12.18 ± 0.23	[c]856	20.54 ± 2.25
1020	1020	6.68 ± 0.62	1021	6.69 ± 0.44				
					1324	211.99 ± 6.80		
							1347	36.66 ± 1.46
1383	1381	2.76 ± 0.12	1382	2.79 ± 0.15				
							1412	78.09 ± 2.33
1463	1463	4.41 ± 0.28	1464	5.50 ± 0.79				
1577	1575	3.68 ± 0.14	1576	3.77 ± 0.07				
					1586	167.71 ± 6.40		
							1596	54.02 ± 4.96
							1799	64.42 ± 1.91
							1920	66.33 ± 1.62
3055	3055	6.22 ± 0.14	3056	4.68 ± 0.03				

Peak = Peak position in cm^{-1}; FWHM = full width half maximum value in cm^{-1}; Initial = PAH as used in the experiment; 21 °C = sample from LTHE at 21 °C; 150 °C = sample from LTHE at 150 °C.
[a]Zhao et al. (2013).
[b]Maddams and Royaud (1990).
[c]Raman bands of olivine.

the bottom after being added to the vial where they stayed without any further visible change throughout the whole experiment.

Figure 7 summarizes the microstructure of the remaining material from naphthalene experiments conducted at temperatures of 80–120 °C. In all cases,

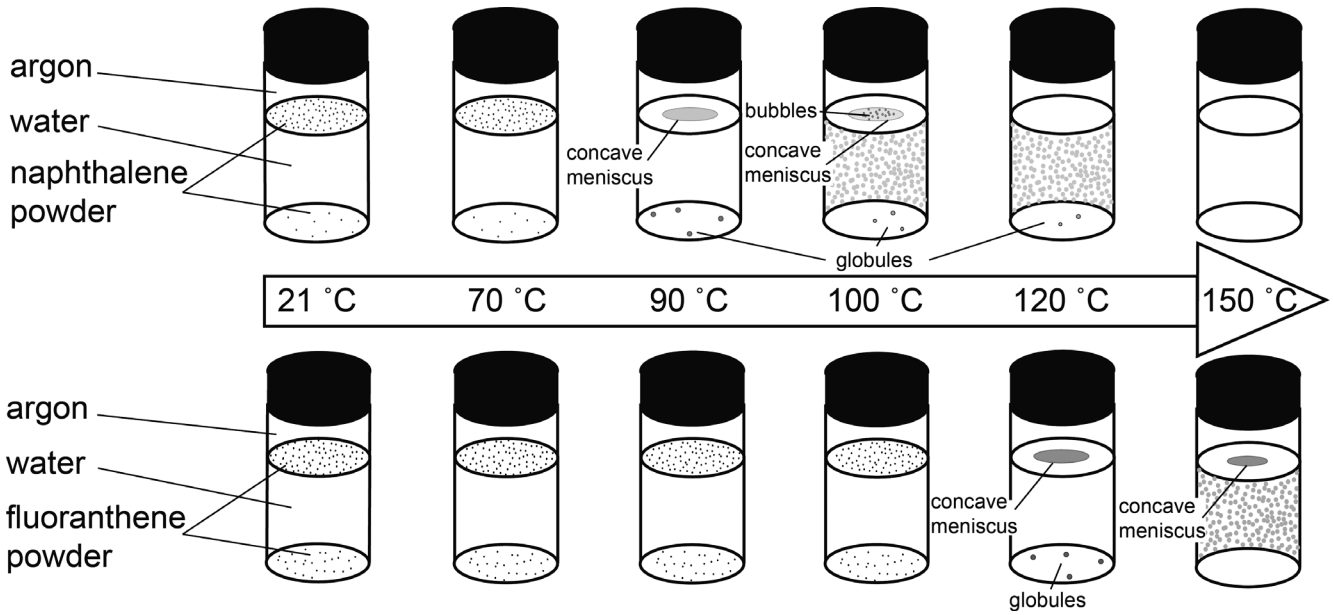

Fig. 6. Macroscopic observations of short-term hydrothermal experiments of naphthalene and fluoranthene with water. Samples were exposed to a temperature profile ranging from room temperature (21 °C) to LTHE temperature (150 °C). Melting points of naphthalene (~80 °C) and fluoranthene (~110 °C) fall within this temperature range (Karcher 1988; Yalkowsky et al. 2010). Both naphthalene and fluoranthene develop a concave meniscus floating on the surface at around 10 °C above their respective melting points. Upon further heating, these menisci shrink, and completely disappear around 30 °C above the melting point for naphthalene, and visibly reduce in size in the fluoranthene experiments around 40 °C above the melting point. At 70 °C above the melting point, naphthalene is no longer visible with the naked eye, leaving a clear fluid.

nanosized spherules aligned to form a string-like network. In contrast to the highly evaporative nature of the naphthalene-derived material, STHE conducted with fluoranthene resulted in carbonaceous material that was stable when subjected to high vacuum conditions. Figure 8 displays a summary of fluoranthene-derived material from experiments ranging between 100 and 150 °C. A few micron-sized cavities developed within the fluoranthene at 100 °C (Fig. 8a), 10 °C below the melting point of fluoranthene (Table 2). These cavities are distributed within the fluoranthene material, and the walls of these cavities occasionally show spherule-like structures. Around 120 °C, the cavities are enlarged with a diameter around 1–3 μm and appear to have more spherules on the walls (Fig. 8b). At 140 °C, 30 °C above the fluoranthene melting point, ring-shaped organic structures develop within small cavities (Figs. 8c–e). Sample material of fluoranthene from STHE conducted at 150 °C shows large cavities filled with elongated, rounded, pillar-like material (Fig. 8f).

Chemical Analysis

The residues from the STHE samples were analyzed with SEM-EDX and Raman spectroscopy. The SEM-EDX measurement of the naphthalene experiments was only possible for the tiny stable fraction that did not evaporate immediately in the SEM vacuum chamber. For naphthalene, fluoranthene, and coronene samples from the STHE, no apparent chemical changes were observed. As for the LTHE, only carbon was measured in the spherules from the STHE with the SEM-EDX. H may also have been present as this is not detectable using EDX. The Raman spectroscopic investigation of naphthalene and coronene samples (see Figure S1 in supporting information) showed no noteworthy change in the Raman band position or FWHM values, indicating no chemical alteration. Fluoranthene samples of the STHE had to be measured by Raman spectroscopy with lower laser intensity to minimize fluorescence (see supporting information) and also showed no indication of alteration. Only samples of naphthalene and fluoranthene up to 120 °C could be measured. Thus, in contrast to the LTHE samples at 150 °C, PAHs from the STHE samples show no spectroscopic evidence for chemical alteration.

DISCUSSION

Aqueous Alteration of PAHs Under Asteroidal Conditions

Large PAHs from the ISM are expected to have been incorporated into asteroids and should be found in meteorites (Plows et al. 2003). However, only small

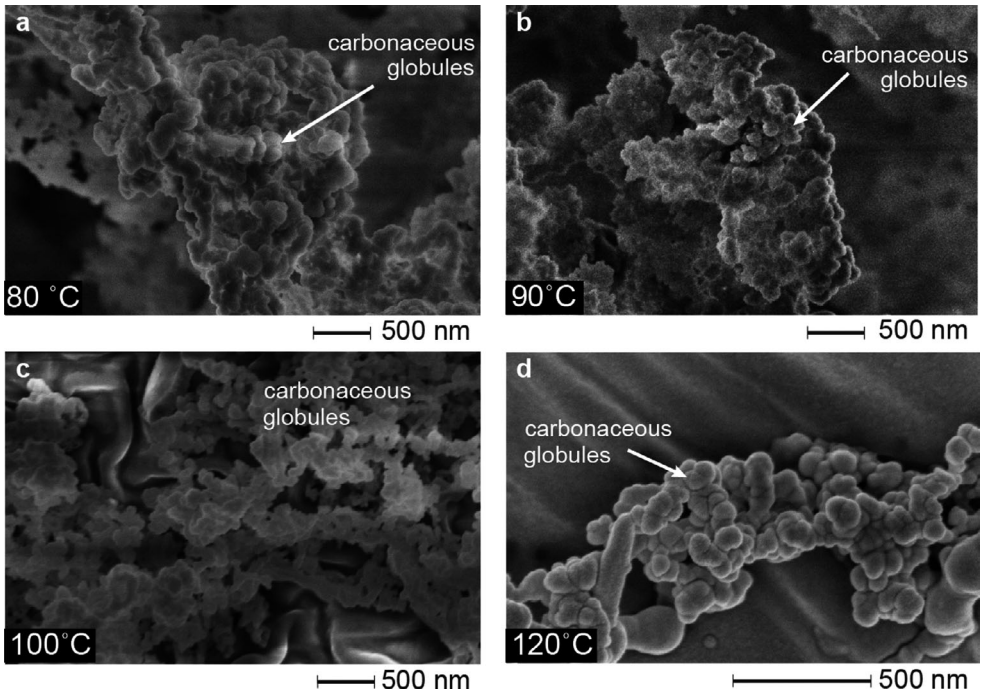

Fig. 7. SEM-FIB images of residual solid material in naphthalene STHEs from 80 to 120 °C. a–d) Carbonaceous globules formed in STHE at 80 °C, 90 °C, 100 °C, and 120 °C, respectively. All four images show string-like material. The string-like material is composed of clusters of carbonaceous globules. The carbonaceous globules show consistent sizes at all investigated temperatures.

PAHs have been found in CCs thus far. In part of our study, we also tested if olivine alteration has an effect on PAHs (e.g., catalyzed breakdown). Alteration of olivine in water can take place within a wide temperature range (Evans 2004), including the aqueous alteration temperatures expected in asteroids (Brearley 2006). It is known that the alteration of olivine supports the alteration of OM in water (Sleep et al. 2004). However, our experiments show that there is no clear link between the aqueous alteration of olivine and the alteration of the tested PAHs.

Our experiments show that, within the aqueous alteration conditions predicted for CCs (Brearley 2006), breakdown of large PAHs into small ones by interactions with water is also unlikely. However, we do observe a chemical change of PAHs near the melting point within the aqueous alteration temperatures predicted for CC. The chemical alteration that occurs via melting was possibly promoted by solvation in water followed by chemical reactions assisted by protonation. Further studies are required to identify the chemical routes and molecular intermediaries involved.

There may be other explanations for the absence of large PAHs in CCs. Large PAHs could have already experienced destruction at a very early stage of their accretion into the parent body (Anderson et al. 2017). Alternatively, large PAHs might still be present as insoluble matter (kerogen) in asteroids and meteorites, respectively (Vinogradoff et al. 2018). In either of these cases, there may be mechanisms for the generation of smaller PAHs that we have not yet discovered, which should be explored in future research.

Organic Spherule Formation by PAHs

PAH derivatives have been suggested to be important in the stabilization of membranous vesicles in aqueous solutions in meteorites (Deamer et al. 2002). Spherule formation from PAHs appears to occur independently of changing chemical environments due to mineral reactivity, modeled using olivine in these experiments. To our knowledge, no published investigation has demonstrated the production of organic spherules by PAHs alone in the presence of aqueous fluids. A successful synthesis of PAH globule structures was reported in the literature during plasma deposition of benzene (C_6H_6) and anthracene ($C_{14}H_{10}$) (Saito and Kimura 2009). Thus, the results of our high-temperature PAH alteration experiments also indicate that spherule formation can occur through the melting of PAHs in water depending on the system temperature.

Our short-term experiments show that spherule formation only occurs in water above specific PAH-dependent temperatures, that is, 90 °C for naphthalene and 120 °C for fluoranthene. These temperatures correlate with the melting temperatures of the PAHs

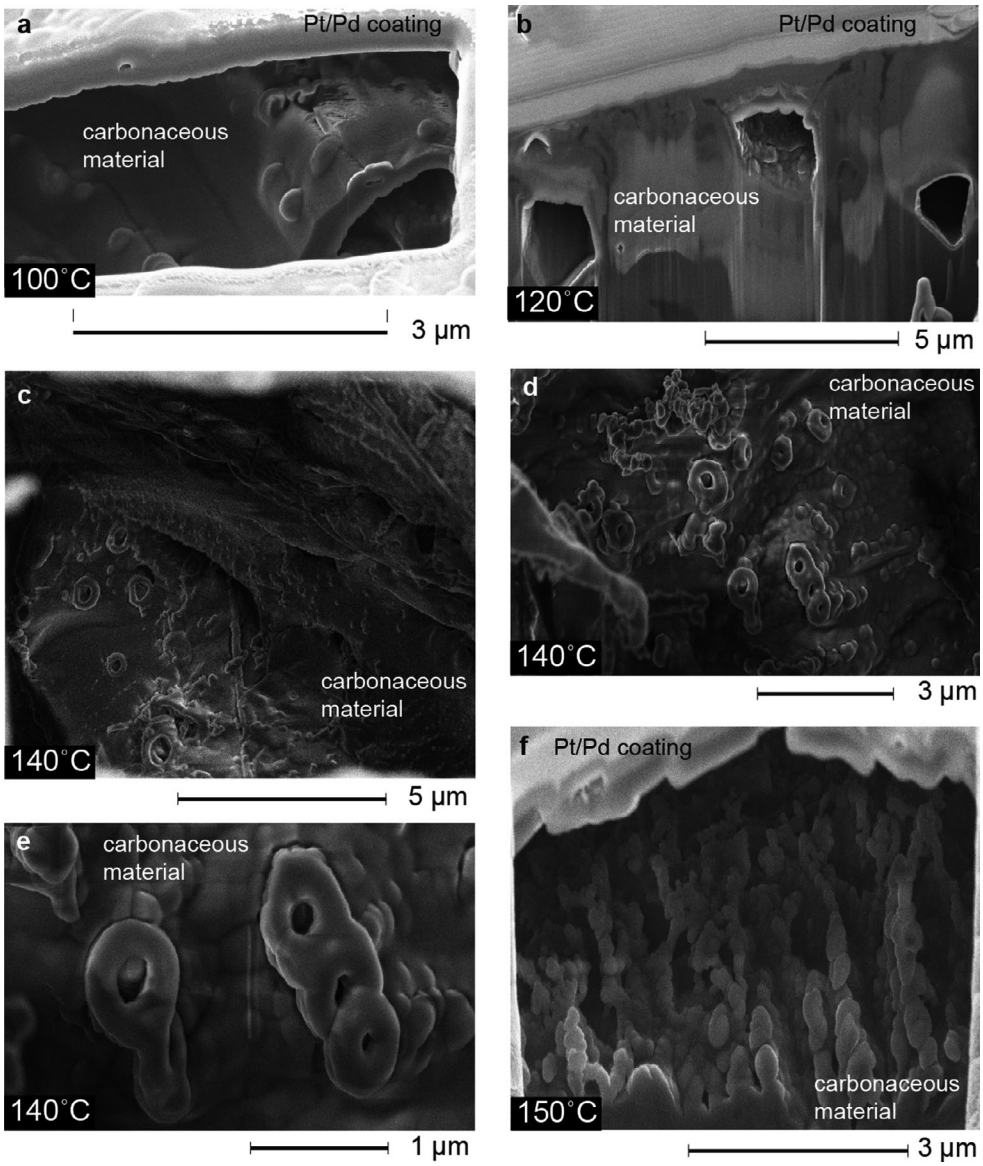

Fig. 8. SEM-FIB images of residual solid material from fluoranthene STHEs, 100–140 °C. a) Solid material formed at 100 °C containing a small cavity at the right lower corner. b) Solid material formed at 120 °C containing several cavities. c–f) Internal structures of cavities formed at 140 and 150 °C, respectively, where the cavity from 150 °C seems to be filled with elongated rounded pillar-like material (f). d and e) Close-up images of a wall within the cavities formed at 140 °C. Several round shape structures are visible.

(Chanyshev et al. 2017), 80–82 °C for naphthalene and 107–110 °C for fluoranthene (Table 2). This observation is also in agreement with the absence of spherule formation in the coronene experiments, as coronene has a melting temperature of 428–440 °C (Chanyshev et al. 2017) (Table 2), far above the highest temperature tested during our experiments.

PAHs are only sparingly soluble in water at room temperature, but their solubility has been shown to increase with increasing temperature (Kus 2012). The PAHs in our experiments are not expected to dissolve significantly into aqueous solutions as the amount of PAH weighed into each sample vessel exceeds the solubility limits (Table 2), even at elevated temperatures (naphthalene: 0.244 g L^{-1} at 73 °C and fluoranthene: 0.017 g L^{-1} at 60 °C; Yalkowsky et al. 2010). An experimental study of benzo(a)pyrene in aqueous solution by Fang and Koziński (2001) demonstrates that even as a melt, PAHs remain insoluble in the aqueous solution until the PAH–water solution becomes supercritical (above the triple point of water). Our experiments are below the supercritical point of water (374 °C; Sengers 2000); thus, the second fluid phase observed in the naphthalene and fluoranthene STHEs is

interpreted as molten PAH. A fraction of naphthalene might also have been lost by sublimation at the air–fluid interface in the experiments above 120 °C in STHE, as an increase in the partial pressure of naphthalene at 150 °C is expected (Fowler et al. 1968; Mackay and Shiu 1977; Macknick and Prausnitz 1979).

The formation of an emulsion, that is, an immiscible PAH melt, in an aqueous solution, helps to explain the formation of the spherule shape in our experiments. For example, crystallization experiments of the organic compound ethylene glycol distearate ($C_{38}H_{74}O_4$; Khalil et al. 2011), which also has low aqueous solubility, form an emulsion with water when molten. These experiments also revealed that solid material often retains the shape of the melt droplets after cooling in an unstirred solution (Khalil et al. 2011). The microstructure produced by the crystallization process of ethylene glycol distearate has parallels with the internal structures observed in the organic spherules produced here. With the fastest cooling rate, ethylene glycol distearate crystallized as dendritic structures in large droplets. Thereby, nucleation occurred both on the interfacial surface between the melt and aqueous solution as well as throughout the droplet bulk. Within the largest droplets produced by fluoranthene in the LTHE (Fig. 4a) and sample material from STHE at 150 °C (Fig. 8), we also observed complex dendrite-like internal structures, indicating a similar formation mechanism as the ethylene glycol distearate dendrites.

In contrast, in the ethylene glycol distearate experiments of Khalil et al. (2011), smaller droplets retained their original size and shape throughout the crystallization process with crystallization only occurring at the droplet edge. Nucleation and growth from the droplet edge in our experiments would explain the hollow and filled structures found in the smaller spherules from the fluoranthene LTHE (Figs. 4g and 4i) as well as the smaller spherules generated in the naphthalene LTHE (Fig. 3). The spherule sizes formed in the naphthalene LTHE at 150 °C show a log-normal distribution (Fig. 5c) indicating homogenous growth (Kile et al. 2000). However, the spherules formed during the LTHE with fluoranthene at 150 °C show an asymptotic size distribution (Fig. 5d). This distribution indicates heterogeneous growth, again consistent with the findings of Khalil et al. (2011) who demonstrate that growth occurs initially in larger droplets of ethylene glycol distearate, with a larger extent of undercooling (temperature below the melting point of ethylene glycol distearate) necessary to initiate crystallization in smaller droplets. The formation of spherules appears to be a common characteristic of insoluble OM, like PAHs, in an aqueous solution after heating above the melting temperature as seen in our results and experiments from Khalil et al. (2011).

Organic Globules in CCs

The first micrometer-sized spherical shapes discovered, hereafter referred to as globules, were found in the Orgueil and Ivuna meteorites and initially interpreted to have been microfossils indigenous to the meteorite, potentially formed by algae (Claus and Nagy 1961) or bacteria (Oró and Tornabene 1965). Today, globules have been found in materials from various environments in the solar system, including interplanetary dust particles (IDPs; Messenger et al. 2008; Busemann et al. 2009), cometary dust (Matrajt et al. 2008; De Gregorio et al. 2010), and as minor components of the insoluble organic fraction in several CCs (Vanlandingham et al. 1967; Rossignol-Strick and Barghoorn 1971; Pflug 1984; Garvie and Buseck 2004, 2006; Nakamura-Messenger et al. 2006; Garvie et al. 2008; Messenger et al. 2008; Clemett et al. 2009; De Gregorio et al. 2010, 2013; Herd et al. 2011; Hashiguchi et al. 2013; Jones 2016; Alexander et al. 2017; Changela et al. 2018).

The globules described in the literature have a diameter size ranging from as small as 50 nm (Garvie and Buseck 2004) up to 340 nm (Rossignol-Strick and Barghoorn 1971). This distribution is replicated in both the spherules from the LTHE and STHE (Figs. 3, 4, 7, and 8) where the largest spherule observed was 50 μm but with the majority of spherules being between 100 and 500 nm. A variety of structures have been observed in CC globules such as double walls (Claus and Nagy 1961; Vanlandingham et al. 1967; Rossignol-Strick and Barghoorn 1971; Pflug 1984) as well as solid or hollow nanospheres (Nakamura et al. 2002; Garvie and Buseck 2004; Nakamura-Messenger et al. 2006; Garvie et al. 2008; Hashiguchi et al. 2013). These structures are also mirrored in the spherules produced in our experiments, particularly in the LTHE with fluoranthene at 150 °C, which produced hollow, filled, and complex structures depending on the spherule size (Figs. 4b, 4c, and 4f). For globules with internal cavities, the wall thickness is reported to be between 2 nm (Pflug 1984) and 100–200 nm (Nakamura et al. 2002; Hashiguchi et al. 2013; Nakamura-Messenger et al. 2013) in CCs. In comparison, the spherule wall thickness produced in our experiments (200 nm on average) fits with the thicknesses found in natural materials, albeit at the smaller end of the size range. Thus, morphologically, the experimentally produced spherules reported here closely resemble the microstructural characteristics of many globules found in CCs indicating that melting of PAHs in water is a potential mechanism for the formation of some organic globules within asteroids.

CCs contain a variety of organic compounds (Sephton et al. 1998; Sephton 2002) spanning a range in

solubility and melting temperatures. Here, we recall that the behavior of naphthalene and fluoranthene in our experiments is characteristic for all organic compounds with limited solubility that are heated above their melting temperature. We expect that such a complex mixture would give rise to a varied composition of the globules formed after heating. We also recognize that different regions of the meteorites may have been heated to different temperatures, and the resulting globules may have been transported in the aqueous environment. We surmise, therefore, that melting and droplet formation may well have played a major role in the formation of globules in the meteoritic parent body. Microspherules have also been produced from other starting materials, such as formaldehyde polymerization (Cody et al. 2011). Therefore, the contribution of melting versus the formation of micelles in aqueous solution, possibly stabilized by PAH derivatives (Deamer et al. 2002), will have to be investigated in future experiments.

The results of the LTHE show that the PAHs have been chemically altered during spherule formation under the chosen experimental conditions (T = 150°C, P = 4.8 bar). This is indicated by the lower vapor pressure of the globule material in air and vacuum in comparison to the starting PAH powders. The change of fluid color in the LTHE samples and the appearance of new Raman bands also indicate that a chemical reaction has taken place. The new Raman bands can still be assigned to aromatic modes, but could not be matched with specific organic molecules. The chemical change may reflect the high proton affinity of PAHs (Chen and Cooks 1995), as compared to H_2O, and efficient formation of protonated PAHs. The charge may assist in polymerization reactions converting small PAHs into larger ones, as well as in cracking reactions and hydrogen transfer (Chanyshev et al. 2017). The results of the STHE do not show the same indications for chemical alteration during spherule formation, which might be explained due to the chosen experimental conditions, including much shorter experiment duration and by not being able to analyze the samples formed at temperatures above 120 °C. However, the samples indicate similar higher stability (high vapor pressure) to that observed from the samples of the LTHE. Therefore, we cannot rule out that chemical changes took place in the STHE samples at 150 °C.

Globule populations in CCs are dominated by organics with a complex mixture of aliphatic and aromatic chemistries. These globules also carry variations in D and ^{15}N isotopic enrichments (e.g., Nakamura et al. 2002; Garvie and Buseck 2004, 2006; De Gregorio et al. 2010). Experiments with D-enriched ice have shown that PAHs can attain isotopic signatures comparable to those observed in meteorites (Sandford et al. 2000). Furthermore, variations of D-enriched PAHs have been detected in several regions of the galaxy, including signatures reflecting D-enriched PAHs in CCs (Peeters et al. 2004; Doney et al. 2016). Our hypothesis may help to explain how D enrichments are retained as the formation of a hydrophobic melt directly from a solid would limit D/H isotopic exchange between the OM and aqueous solution. Based on our hypothesis, PAHs with a ^{15}N anomaly could have also retained their isotopic signature during globule formation from sparingly soluble material, such as PAHs, via an emulsion in aqueous solution. So far, however, no single formation mechanism has been proposed to explain all of the observed characteristics of these globules, suggesting that their properties are a result of multiple processes occurring in a variety of environments (Alexander et al. 1998; De Gregorio et al. 2013). In this regard, we emphasize that our proposed mechanism for the formation of globules with a PAH chemistry is linked to aqueous environments and hence does not address globule formation in solar system materials that have not seen liquid water such as comets and IDPs.

A Potential Link Between Globules and PAH Solubility

Nakamura-Messenger et al. (2006) proposed that aqueous alteration in the parent body of the Tagish Lake meteorite might be a possible mechanism for carbonaceous globule formation. It is evident from our experiments that PAHs in aqueous solution can form solid spherules when an emulsion is formed and that these spherules can replicate the size and internal structure of globules that have been found in CCs. The aqueous alteration would have occurred at elevated temperatures due to ^{26}Al decay (Urey 1955; Fuse and Anders 1969). Figure 9 shows that the estimated aqueous alteration conditions for different CC meteorite groups overlain with the melting temperatures of different PAH molecules based on the number of their C atoms. This plot demonstrates that all of the meteorite CC groups, with the exception of CO meteorites, are expected to have seen aqueous alteration above the melting temperatures of naphthalene and fluoranthene. However, for such a mechanism to be active on a meteorite parent body, one needs to evaluate whether there will be sufficient concentrations of PAHs to surpass the solubility limit under the conditions of aqueous alteration. Taking the Allende meteorite as an example, with a water content of 0.2 wt% (Jarosewich et al. 1987) and 0.055–2 ppm naphthalene (Zenobi et al. 1989), the naphthalene concentration ranges between 10^{-5} and 10^{-3} mg g^{-1}. This is below naphthalene's solubility in water (0.031 g L^{-1}; Yalkowsky et al. 2010).

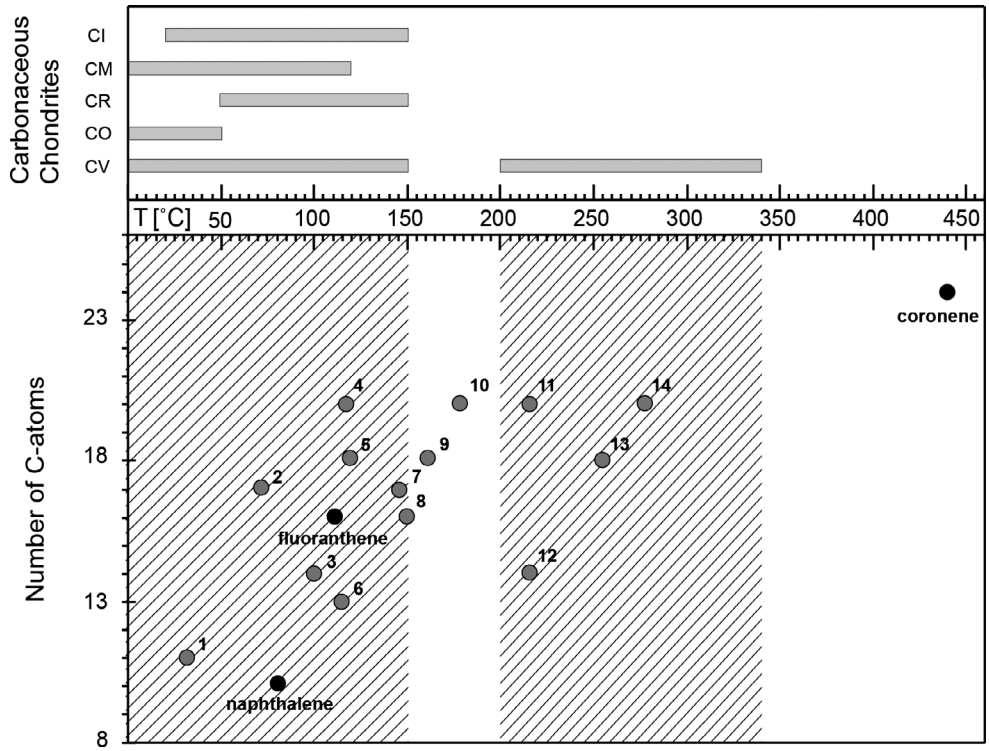

Fig. 9. Melting points of PAHs detected in carbonaceous chondrites and aqueous alteration temperature ranges of carbonaceous chondrites. The plot shows the overlap of PAH melting points (gray and black dots; data form Karcher [1988] and Haynes [2012]) and the aqueous alteration temperature ranges of carbonaceous chondrites (gray bars; summarized: dashed areas; data from Brearley 2006). Comparing PAH melting temperatures with aqueous meteorite alteration conditions suggests that carbon globules may form as a result of PAH melting during meteorite alteration. It also indicates that remnant coronene, detected on meteorites, was not able to form globules as the melting point lies outside the aqueous alteration temperature. The following PAHs have been detected in carbonaceous chondrites: napthalene (a–c), flyoranthene (a–e), coronene (b, e), (1) 2-methylnaphthalene (a), (2) 1-methylpyrene (d), (3) phenanthrene (a–f), (4) benzo(c)fluorine (d, e), (5) benzo(cgi)fluoranthene (d), (6) fluorene (b, d), (7) 20methylpyrene (d), (8) pyrene (a–f), (9) benz(a)anthracene (d), (10) benzo(a)pyrene, benzo(e)pyrene (b, d, e), (11) benzo(b)fluorene (d, e), (12) anthracene (b, d, e), (13) chyrsene (d, e, f), (14) perylene (b, d, e) (a: Plows et al. 2003; b: Zenobi et al. 1989; c: Hahn et al. 1988; d: Basile et al. 1984; e: de Vries et al. 1993; f: Clemett et al. 2009).

On Earth, PAHs are preferentially partitioned onto solid particles due to their low solubility (Wilcke 2000). Similarly, PAHs in meteorite parent bodies are expected to be situated on/at mineral surfaces/interfaces. This is consistent with observations that PAHs are not homogeneously distributed within meteorites, as indicated by Zenobi et al. (1989). Heating may also have been localized (De Gregorio et al. 2010) causing an uneven distribution of water within the parent body (Brearley 2006). Dissolution into smaller fluid reservoirs would result in higher PAH concentrations in solution. Given the very low solubilities of PAHs, accumulation of PAHs into smaller reservoirs should thus allow PAH aggregates to surpass their aqueous solubility thus facilitating melt formation within these reservoirs.

PAH solubility decreases with increasing salinity (Gold and Rodriguez 1989) but increases with increasing temperature (Yalkowsky et al. 2010). Thus, the maximum concentration required for PAHs to surpass their saturation would be dependent on the alteration conditions. Although the elevated temperatures during alteration would increase PAH solubility, the extensive mineral alteration products (e.g., salts) indicate that ions should be present in the aqueous solution, which could have a counter effect. The composition of the solution does not appear to influence PAH dissolution (Giese et al. 2018); hence, increasing ionic strength would thus compensate for increasing solubility at higher temperatures, again facilitating the formation of globules via melting. Therefore, it seems that globule formation by PAH melting under asteroidal conditions is likely and could contribute to the variety of globules found in CCs.

CONCLUSION

In this study, we investigated the aqueous alteration of PAHs under asteroidal parent body conditions. In our

experiments, we exposed three PAHs (naphthalene [$C_{10}H_8$], fluoranthene [$C_{16}H_{10}$], and coronene [$C_{24}H_{12}$]) in water to increasing temperatures and pressures. Raman spectroscopy indicates that the small PAHs tested (up to 16 carbon atoms) may be chemically altered, unlike the larger PAH examined in our experiments. Our experiments also show that there is no clear link between the aqueous alteration of olivine and the alteration of the tested PAHs. This suggests that aqueous alteration will not convert larger ISM-formed and more stable PAHs (e.g., coronene) into smaller PAHs.

The main result of our study is that naphthalene and fluoranthene produced spherules that are strikingly similar in shape, internal structure, and size to many globules found in CCs. In contrast, in the experiments with coronene, no spherules were formed. We considered a correlation between spherule formation and melting temperature of the PAHs. Based on this correlation, we suggest that the formation of an emulsion of small PAHs and the aqueous solution is a globule-forming mechanism. This is consistent with the overlap of PAH melting temperatures with predicted aqueous alteration conditions for CCs. The melting points of naphthalene and fluoranthene lie within the aqueous alteration conditions of CCs, whereas that of coronene lies outside these conditions. Thus, larger PAHs would not be expected to melt and form spherules. Khalil et al. (2011) show in their experiments that the formation of spherules seems to be a common characteristic of organic material with very low solubility in an aqueous solution after heating above the melting temperature.

Further studies will have to be performed to address the characteristics of globules formed from complex organic mixtures. Our proposed hypothesis for globule formation could also be translated to other OM as long as they are above the solution saturation limit and have similar chemical and physical properties to PAHs. The effect of PAHs with altered or more complex chemistries, reflecting the composition of the observed globules in CCs, also needs to be explored as changes in solubility and melting point due to differences in chemistry will play an important role in the formation of globules through melting. It is not yet clear whether the melting mechanism is present in nature. Globule structures can be generated prior to the meteorite parent body formation, as proposed by Jones (2016); however, whether these globules can be retained is unclear. Similarly, spherules have also been produced experimentally in aqueous solution from formaldehyde polymerization (Cody et al. 2011). Spatially resolved, in situ investigations of PAH concentration variability in CCs will help to establish whether the PAHs can exceed their solubility limit during aqueous alteration on different parent bodies, or if they can be completely dissolved into the aqueous solution as suggested by Wing and Bada (1991). Our proposed mechanism for the formation of globules with a PAH chemistry may explain how D and ^{15}N-enrichments can be retained in globules if isotopic signatures are imprinted prior to parent body formation. However, the effect of melting on the isotopic signatures associated with the globules warrants further investigation.

Acknowledgment—We thank the anonymous reviewer and Dr. Joseph Nuth for their helpful and constructive comments that greatly contributed to improving the final version of the paper. We also thank Editor, Dr. Scott Sandford, for his comments and support during the review process. This project was funded by Spinoza prize awarded to Prof. Dr. Xander Tielens. The experiments and analytical work were conducted at University of Bonn and at Utrecht University. We thank our colleagues Tilly Bouten and Dr. Serguei Matveev for assistance with scanning electron microscopic analyses.

Editorial Handling—Dr. Scott Sandford

REFERENCES

Alajtal A., Edwards H., Elbagerma M., and Scowen I. 2010. The effect of laser wavelength on the Raman spectra of phenanthrene, chrysene, and tetracene: Implications for extra-terrestrial detection of polyaromatic hydrocarbons. *Spectrochimica Acta Part A: Molecular and Biomolecular Spectroscopy* 76:1–5.

Alexander C. M. O'D., Russell S. S., Arden J. W., Ash R. D., Grady M. M., and Pillinger C. T. 1998. The origin of chondritic macromolecular organic matter: A carbon and nitrogen isotope study. *Meteoritics & Planetary Science* 334:603–622.

Alexander C. O'D., Cody G., De Gregorio B., Nittler L., and Stroud R. 2017. The nature, origin and modification of insoluble organic matter in chondrites, the major source of Earth's C and N. *Chemie der Erde-Geochemistry* 77:227–256.

Allamandola L. J., Tielens A. G. G. M., and Barker J. R. 1985. Polycyclic aromatic hydrocarbons and the unidentified infrared emission bands: Auto exhaust along the Milky Wayexclamation. *The Astrophysical Journal* 290: L25–L28.

Anderson D. E., Bergin E. A., Blake G. A., Ciesla F. J., Visser R., and Lee J.-E. 2017. Destruction of refractory carbon in protoplanetary disks. *The Astrophysical Journal* 845:13.

Auwers K. V. and Frühling A. 1921. Über die Spektrochemie mehrkerniger aromatischer Verbindungen und die Konstitution des Naphthalins. *Justus Liebigs Annalen der Chemie* 422:92–230.

Basile B. P., Middleditch B. S., and Oró J. 1984. Polycyclic aromatic hydrocarbons in the Murchison meteorite. *Organic Geochemistry* 54:211–216.

Becker L. and Bunch T. E. 1997. Fullerenes, fulleranes and polycyclic aromatic hydrocarbons in the Allende meteorite. *Meteoritics & Planetary Science* 32:479–487.

Botta O. and Bada J. L. 2002. Extraterrestrial organic compounds in meteorites. *Surveys in Geophysics* 23:411–467.

Brearley A. J. 2006. The action of water. In *Meteorites and the early solar system II*, edited by Lauretta D. S., and McSween H. Y. J. Tucson, Arizona: University of Arizona Press. pp. 584–624.

Bunch T. E. and Chang S. 1980. Carbonaceous chondrites—II. Carbonaceous chondrite phyllosilicates and light element geochemistry as indicators of parent body processes and surface conditions. *Geochimica et Cosmochimica Acta* 44:1543–1577.

Buseck P. R. and Hua X. 1993. Matrices of carbonaceous chondrite meteorites. *Annual Review of Earth and Planetary Sciences* 21:255–305.

Busemann H., Nguyen A. N., Cody G. D., Hoppe P., Kilcoyne A. L. D., Stroud R. M., Zega T. J., and Nittler L. R. 2009. Ultra-primitive interplanetary dust particles from the comet 26P/Grigg–Skjellerup dust stream collection. *Earth and Planetary Science Letters* 288:44–57.

Changela H. G., Le Guillou C., Bernard S., and Brearley A. J. 2018. Hydrothermal evolution of the morphology, molecular composition, and distribution of organic matter in CR Renazzo-type chondrites. *Meteoritics & Planetary Science* 535:1006–1029.

Chanyshev A. D., Litasov K. D., Shatskiy A. F., Sharygin I. S., Higo Y., and Ohtani E. 2017. Transition from melting to carbonization of naphthalene, anthracene, pyrene and coronene at high pressure. *Physics of the Earth and Planetary Interiors* 270:29–39.

Chen G. and Cooks R. G. 1995. Electron affinities of polycyclic aromatic hydrocarbons determined by the kinetic method. *Journal of Mass Spectrometry* 30:1167–1173.

Chirico R. D., Knipmeyer S. E., Nguyen A., and Steele W. V. 1993. The thermodynamic properties to the temperature 700 K of naphthalene and of 2,7-dimethylnaphthalene. *The Journal of Chemical Thermodynamics* 25:1461–1494.

Claus G. and Nagy B. 1961. A microbiological examination of some carbonaceous chondrites. *Nature* 192:594–596.

Clemett S. J., Dulay M. T., Gillette J. S., Chillier X. D. F., Mahajan T. B., and Zare R. N. 1998. Evidence for the extraterrestrial origin of polycyclic aromatic hydrocarbons in the Martian meteorite ALH84001. *Faraday Discuss* 109:417–436.

Clemett S. J., Nakamura-Messenger K., Messenger S., and Thomas-Keprta K. L. 2009. Molecular composition of carbonaceous globules in the Bells CM2 chondrite (abstract). 72nd Annual Meeting of the Meteoritical Society 5445.

Cody G. D., Heying E., Alexander C. M. O., Nittler L. R., Kilcoyne A. L. D., Sandford S. A., and Stroud R. M. 2011. Establishing a molecular relationship between chondritic and cometary organic solids. *Proceedings of the National Academy of Sciences* 108:19,171–19,176.

Colangeli L., Mennella V., Baratta G., Bussoletti E., and Strazzulla G. 1992. Raman and infrared spectra of polycyclic aromatic hydrocarbon molecules of possible astrophysical interest. *The Astrophysical Journal* 396:369–377.

Deamer D., Dworkin J. P., Sandford S. A., Bernstein M. P., and Allamandola L. J. 2002. The first cell membranes. *Astrobiology* 2:371–381.

De Gregorio B., Stroud R., Nittler L., Alexander C., Kilcoyne A., and Zega T. 2010. Isotopic anomalies in organic nanoglobules from comet 81P/Wild 2: Comparison to Murchison nanoglobules and isotopic anomalies induced in terrestrial organics by electron irradiation. *Geochimica et Cosmochimica Acta* 74:4454–4470.

De Gregorio B. T., Stroud R. M., Nittler L. R., Alexander C. M. O'D., Bassim N. D., Cody G. D., Kilcoyne A. L. D., Sandford S. A., Milam S. N., Nuevo M., and Zega T. J. 2013. Isotopic and chemical variation of organic nanoglobules in primitive meteorites. *Meteoritics & Planetary Science* 48:904–928.

De Vries M. S., Reihs K., Wendt H. R., Golden W. G., Hunziker H. E., Fleming R., Peterson E., and Chang S. 1993. A search for C60 in carbonaceous chondrites. *Geochimica et Cosmochimica Acta* 57:933–938.

Doney K. D., Candian A., Mori T., Onaka T., and Tielens A. 2016. Deuterated polycyclic aromatic hydrocarbons: Revisited. *Astronomy & Astrophysics* 586:A65.

Elsila J. E., de Leon N. P., Buseck P. R., and Zare R. N. 2005. Alkylation of polycyclic aromatic hydrocarbons in carbonaceous chondrites. *Geochimica et Cosmochimica Acta* 69:1349–1357.

Evans B. W. 2004. The serpentinite multisystem revisited: Chrysotile is metastable. *International Geology Review* 46:479–506.

Evans B. W., Hattori K., and Baronnet A. 2013. Serpentinite: What, why, where? *Elements* 9:99–106.

Fang Z. and Koziński J. A. 2001. Phase changes of benzo a pyrene in supercritical water combustion. *Combustion and Flame* 1241:255–267.

Fiedler H., Mertens C., Morgenstern M., Scheidt M., and Hutzinger O. 1997. Fluoranthen. In *Stoffverhalten von Gaswerkspezifischen Polycyclischen Aromatischen Kohlenwasserstoffen Saparpakorn et al*. Mannheim: Landesamt für Umweltschutz Baden-Württemberg. pp. 72–75.

Fowler L., Trump W. N., and Vogler C. E. 1968. Vapor pressure of naphthalene. Measurements between 40° and 180°. *Journal of Chemical & Engineering Data* 13:209–210.

Fuse K. and Anders E. 1969. Aluminum-26 in meteorites—VI Achondrites. *Geochimica et Cosmochimica Acta* 336:653–670.

Garvie L. A. J. and Buseck P. R. 2004. Nanosized carbon-rich grains in carbonaceous chondrite meteorites. *Earth and Planetary Science Letters* 224:431–439.

Garvie L. A. J. and Buseck P. R. 2006. Carbonaceous materials in the acid residue from the Orgueil carbonaceous chondrite meteorite. *Meteoritics & Planetary Science* 41:633–642.

Garvie L. A. J., Baumgardner G., and Buseck P. R. 2008. Scanning electron microscopical and cross sectional analysis of extraterrestrial carbonaceous nanoglobules. *Meteoritics & Planetary Science* 43:899–903.

Giese C.-C., King H. E., van den Ende M. P. A., Plümper O., ten Kate I. L., and Tielens A. G. G. M. 2018. In situ nanoscale investigation of step retreat on fluoranthene crystal surfaces. *ACS Earth and Space Chemistry* 2:1301–1311.

Gold G. and Rodriguez S. 1989. The effect of temperature and salinity on the Setschenow parameters of naphthalene in seawater. *Canadian Journal of Chemistry* 67:822–826.

Hahn J. H., Zenobi R., Bada J. L., and Zare R. N. 1988. Application of two-step laser mass spectrometry to cosmogeochemistry: Direct analysis of meteorites. *Science* 239:1523–1525.

Hashiguchi M., Kobayashi S., and Yurimoto H. 2013. In situ observation of D-rich carbonaceous globules embedded in NWA 801 CR45 chondrite. *Geochimica et Cosmochimica Acta* 122:306–323.

Herd C. D., Blinova A., Simkus D. N., Huang Y., Tarozo R., Alexander C. M., Gyngard F., Nittler L. R., Cody G. D., Fogel M. L., Kebukawa Y., Kilcoyne A. L., Hilts R. W., Slater G. F., Glavin D. P., Dworkin J. P., Callahan M. P., Elsila J. E., De Gregorio B. T., and Stroud R. M. 2011. Origin and evolution of prebiotic organic matter as inferred from the Tagish Lake meteorite. *Science* 332:1304–1307.

Ishitani T. and Yaguchi T. 1996. Cross-sectional sample preparation by focused ion beam: A review of ion-sample interaction. *Microscopy Research and Technique* 354:320–333.

Jarosewich E., Clarke R. S. Jr, and Barrows J. N. 1987. Allende meteorite reference sample. *Smithsonian Contributions to the Earth Sciences*.

Jones A. P. 2016. Dust evolution, a global view: III. Core/mantle grains, organic nano-globules, comets and surface chemistry. *Royal Society Open Science* 3:160–224.

Karcher W. 1988. *Spectral atlas of polycyclic aromatic compounds*, vol. 2. Dordrecht: Kluwer Academic Publishers. p. 880.

Kell G. S. 1975. Density, thermal expansivity, and compressibility of liquid water from 0° to 150°. Correlations and tables for atmospheric pressure and saturation reviewed and expressed on 1968 temperature scale. *Journal of Chemical & Engineering Data* 20:97–105.

Khalil A., Puel F., Cosson X., Gorbatchev O., Chevalier Y., Galvan J.-M., Rivoire A., and Klein J.-P. 2011. Crystallization-in-emulsion process of a melted organic compound: In situ optical monitoring and simultaneous droplet and particle size measurements. *Journal of Crystal Growth* 342:99–109.

Kile D. E., Eberl D. D., Hoch A. R., and Reddy M. M. 2000. An assessment of calcite crystal growth mechanisms based on crystal size distributions. *Geochimica et Cosmochimica Acta* 64:2937–2950.

Kus N. S. 2012. Organic reactions in subcritical and supercritical water. *Tetrahedron* 68:949–958.

Le Guillou C., Bernard S., Brearley A. J., and Remusat L. 2014. Evolution of organic matter in Orgueil, Murchison and Renazzo during parent body aqueous alteration: In situ investigations. *Geochimica et Cosmochimica Acta* 131:368–392.

Lin-Vien D., Colthup N. B., Fateley W. G., and Grasselli J. G. 1991. *The handbook of infrared and Raman characteristic frequencies of organic molecules*. London: Academic Press.

Liu Y., King H. E., van Huis M. A., Drury M. R., and Plümper O. 2016. Nano-tomography of porous geological materials using focused ion beam-scanning electron microscopy. *Minerals* 6:104.

Mackay D. and Shiu W. Y. 1977. Aqueous solubility of polynuclear aromatic hydrocarbons. *Journal of Chemical & Engineering Data* 22:399–402.

Macknick A. B. and Prausnitz J. M. 1979. Vapor pressures of high-molecular-weight hydrocarbons. *Journal of Chemical & Engineering Data* 24:175–178.

Maddams W. and Royaud I. 1990. The characterization of polycyclic aromatic hydrocarbons by Raman spectroscopy. *Spectrochimica Acta Part A: Molecular Spectroscopy* 462:309–314.

Matrajt G., Ito M., Wirick S., Messenger S., Brownlee D. E., Joswiak D., Flynn G., Sandford S., Snead C., and Westphal A. 2008. Carbon investigation of two Stardust particles: A TEM, NanoSIMS, and XANES study. *Meteoritics & Planetary Science* 43:315–334.

Messenger S., Nakamura-Messenger K., and Keller L. P. 2008. N-15-rich organic globules in a cluster IDP and the bells CM2 chondrite. 39th Lunar and Planetary Science Conference. CD-ROM.

Nakamura K., Zolensky M. E., Tomita S., Nakashima S., and Tomeoka K. 2002. Hollow organic globules in the Tagish Lake meteorite as possible products of primitive organic reactions. *International Journal of Astrobiology* 1:179–189.

Nakamura-Messenger K., Messenger S., Keller L. P., Clemett S. J., and Zolensky M. E. 2006. Organic GLOBULES in the Tagish Lake meteorite: Remnants of the protosolar disk. *Science* 314:1439–1442.

Nakamura-Messenger K., Messenger S., Keller L. P., Clemett S. J., Nguyen A. N., and Gibson E. K.. 2013. Coordinated in situ analyses of organic nanoglobules in the Sutter's mill meteorite (abstract). 44th Lunar and Planetary Science Conference. CD-ROM.

Nasdala L., Irmer G., and Wolf D. 1995. The degree of metamictization in zircons: A Raman spectroscopic study. *European Journal of Mineralogy-Ohne Beihefte* 7:471–478.

Oró J. and Tornabene T. 1965. Bacterial contamination of some carbonaceous meteorites. *Science* 150:1046–1048.

Peeters E., Allamandola L. J., Bauschlicher J. C. W., Hudgins D. M., Sandford S. A., and Tielens A. G. G. M. 2004. Deuterated interstellar polycyclic aromatic hydrocarbons. *The Astrophysical Journal* 604:252–257.

Pflug H. D. 1984. Microvesicles in meteorites, a model of prebiotic evolution. *Naturwissenschaften* 71:531–533.

Plows F. L., Elsila J. E., Zare R. N., and Buseck P. R. 2003. Evidence that polycyclic aromatic hydrocarbons in two carbonaceous chondrites predate parent-body formation. *Geochimica et Cosmochimica Acta* 67:1429–1436.

Ram S., Pandey V., and Thakur S. 1983. Infrared and Raman studies of some naphthols. *Pramana* 20:163–174.

Ross R. G., Andersson P., and Bäckström G. 1979. Thermal conductivity and heat capacity of benzene, naphthalene and anthracene under pressure. *Molecular Physics* 382:527–533.

Rossignol-Strick M. and Barghoorn E. S. 1971. Extra terrestrial abiogenic organization of organic matter: The hollow spheres of the Orgueil meteorite. *Space Life Sciences* 3:89–107.

Saito M. and Kimura Y. 2009. Origin of organic globules in meteorites: Laboratory simulation using aromatic hydrocarbons. *The Astrophysical Journal* 703:L147–L151.

Sandford S. A., Bernstein M. P., Allamandola L. J., Gillette J. S., and Zare R. N. 2000. Deuterium enrichment of polycyclic aromatic hydrocarbons by photochemically induced exchange with deuterium-rich cosmic ices. *The Astrophysical Journal* 538:691–697.

Schaeffer M. W., Kim W., Maxton P. M., Romascan J., and Felker P. M. 1995. Raman spectroscopy of naphthalene clusters. Evidence for a symmetrical trimer and an unsymmetrical tetramer. *Chemical Physics Letters* 242:632–638.

Schulte M. and Shock E. 2004. Coupled organic synthesis and mineral alteration on meteorite parent bodies. *Meteoritics & Planetary Science* 399:1577–1590.

Sengers J. M. H. L. 2000. Supercritical fluids: Their properties and applications. In *Supercritical fluids: Fundamentals and*

applications., edited by Kiran E., Debenedetti P. G., and Peters C. J. Dordrecht: Springer, the Netherlands: Springer. pp. 1–29.
Sephton M. A. 2002. Organic compounds in carbonaceous meteorites. *Natural Product Reports* 19:292–311.
Sephton M. A., Pillinger C. T., and Gilmour I. 1998. δ13C of free and macromolecular aromatic structures in the murchison meteorite. *Geochimica et Cosmochimica Acta* 6210:1821–1828.
Shinohara H., Yamakita Y., and Ohno K. 1998. Raman spectra of polycyclic aromatic hydrocarbons. Comparison of calculated Raman intensity distributions with observed spectra for naphthalene, anthracene, pyrene, and perylene. *Journal of Molecular Structure* 442:221–234.
Sleep N. H., Meibom A., Fridriksson T., Coleman R. G., and Bird D. K. 2004. H_2-rich fluids from serpentinization: Geochemical and biotic implications. *Proceedings of the National Academy of Sciences* 101:12,818–12823.
Tan X., Chen X., and Song S. 2017. A computational study of spectral matching algorithms for identifying Raman spectra of polycyclic aromatic hydrocarbons. *Journal of Raman Spectroscopy* 48:113–118.
Tielens A. G. 2008. Interstellar polycyclic aromatic hydrocarbon molecules. *Annual Review of Astronomy and Astrophysics* 46:289–337.
Urey H. C. 1955. The cosmic abundances of potassium, uranium, and thorium and the heat balances of the Earth, the Moon, and Mars. *Proceedings of the National Academy of Sciences of the United States of America* 41:127.
Vanlandingham S. L., Sun C. N., and Tan W. C. 1967. Origin of round-body structures in the orgueil meteorite. *Nature* 216:252–253.
Vinogradoff V., Bernard S., Le Guillou C., and Remusat L. 2018. Evolution of interstellar organic compounds under asteroidal hydrothermal conditions. *Icarus* 305:358–370.
Volkert C. A. and Minor A. M. 2011. Focused ion beam microscopy and micromachining. *MRS Bulletin* 325:389–399.
Weisberg M. K., McCoy T. J., and Krot A. N. 2006. Systematics and evaluation of meteorite classification. In *Meteorites and the early solar system II*, edited by Lauretta D. S. and McSween H. R. Jr. Tucson, Arizona: University of Arizona Press. pp. 19–52.
Wilcke W. 2000. SYNOPSIS polycyclic aromatic hydrocarbons PAHs in soil—A review. *Journal of Plant Nutrition and Soil Science* 1633:229–248.
Wing M. R. and Bada J. L. 1991. The origin of the polycyclic aromatic hydrocarbons in meteorites. *Origins of Life and Evolution of the Biosphere* 21:375–383.
Yalkowsky S. H., He Y., and Jain P. 2010. Solubility data. In *Handbook of aqueous solubility data*, 2nd ed. Boca Raton, Florida: CRC Press. pp. 1–1366.
Zenobi R., Philippoz J.-M., Buseck P. R., and Zare R. N. 1989. Spatially resolved organic analysis of the Allende meteorite. *Science* 246:1026–1029.
Zhao X.-M., Zhang J., Berlie A., Qin Z.-X., Huang Q.-W., Jiang S., Zhang J.-B., Tang L.-Y., Liu J., and Zhang C. 2013. Phase transformations and vibrational properties of coronene under pressure. *The Journal of Chemical Physics* 139:144,308.
Zolensky M. E. 2005. Extraterrestrial water. *Elements* 1:39–43.

SUPPORTING INFORMATION

Additional supporting information may be found in the online version of this article:

Figure S1. Raman spectra of short-term hydrothermal experiment (STHE). (a) Raman spectra of naphthalene exposed to water from room temperature till 120 °C in STHE. (b) Raman spectra of fluoranthene exposed to water from room temperature till 120 °C in STHE. (a) Raman spectra of coronene exposed to water from room temperature till 150 °C in STHE. The spectra obtained from the samples do not show any alteration.